Clim. Past, 7, 869–880, 2011
www.clim-past.net/7/869/2011/
doi:10.5194/cp-7-869-2011

Climate of the Past

Antarctic ice sheet and oceanographic response to eccentricity forcing during the early Miocene

D. Liebrand[1,2], L. J. Lourens[1], D. A. Hodell[3], B. de Boer[4], R. S. W. van de Wal[4], and H. Pälike[2]

[1]Department of Earth Sciences, Faculty of Geosciences, Utrecht University, Budapestlaan 4, 3584 CD Utrecht, The Netherlands
[2]School of Ocean and Earth Science, University of Southampton, National Oceanography Centre, Southampton, European Way, Southampton, SO14 3ZH, UK
[3]Department of Earth Sciences, University of Cambridge, Downing Street, Cambridge, CB2 3EQ, UK
[4]Institute for Marine and Atmospheric research Utrecht (IMAU), Utrecht University, Princetonplein 5, 3584 CC Utrecht, The Netherlands

Received: 15 November 2010 – Published in Clim. Past Discuss.: 20 December 2010
Revised: 30 June 2011 – Accepted: 13 July 2011 – Published: 12 August 2011

Abstract. Stable isotope records of benthic foraminifera from ODP Site 1264 in the southeastern Atlantic Ocean are presented which resolve the latest Oligocene to early Miocene (∼24–19 Ma) climate changes at high temporal resolution (<3 kyr). Using an inverse modelling technique, we decomposed the oxygen isotope record into temperature and ice volume and found that the Antarctic ice sheet expanded episodically during the declining phase of the long-term (∼400 kyr) eccentricity cycle and subsequent low short-term (∼100 kyr) eccentricity cycle. The largest glaciations are separated by multiple long-term eccentricity cycles, indicating the involvement of a non-linear response mechanism. Our modelling results suggest that during the largest (Mi-1) event, Antarctic ice sheet volume expanded up to its present-day configuration. In addition, we found that distinct ∼100 kyr variability occurs during the termination phases of the major Antarctic glaciations, suggesting that climate and ice-sheet response was more susceptible to short-term eccentricity forcing at these times. During two of these termination-phases, δ^{18}O bottom water gradients in the Atlantic ceased to exist, indicating a direct link between global climate, enhanced ice-sheet instability and major oceanographic reorganisations.

Correspondence to: D. Liebrand
(diederik.liebrand@noc.soton.ac.uk)

1 Introduction

Earth's climate has gradually cooled during the past 50 million years in conjunction with declining atmospheric pCO_2 conditions (Zachos et al., 2008). Following the cooling and rapid expansion of Antarctic continental ice-sheets in the earliest Oligocene, deep-sea oxygen isotope (δ^{18}O) values remained relatively heavy (2.5 ‰), indicating permanent ice cover with a mass as large as 50 % of that of the present-day and bottom-water temperatures of ∼4 °C (Lear et al., 2004). The Antarctic ice sheets reduced in size during the course of the Oligocene and early Miocene excepting several brief periods of glaciation. One such glaciation is the Mi-1 episode/zone (Miller et al., 1991), which encompasses the Oligocene-Miocene transition. Initially, only two Oligocene and six Miocene oxygen isotope zones (Oi-1, Oi-2, Mi-1 – Mi-6) were described (Miller et al., 1991). Several smaller glaciations were later identified in isotope records spanning the latest Oligocene and early Miocene and were labeled Mi-1a, Mi-1b, Mi-7, Mi-1aa (Wright and Miller, 1992), Oi-2b.1, Mi-1.1 (Billups et al., 2002) and one still unnamed zone (Paul et al., 2000). It has long been suspected that the large-scale changes in Antarctic ice volume are coupled to long-term eccentricity (2.0–2.6 Myr) and obliquity (∼1.2 Myr) modulations of the Earth's orbit and axial tilt (Miller et al., 1991; Wright and Miller, 1992; Beaufort, 1994; Lourens and Hilgen, 1997). But, this theory could only recently be tested through the generation of high-resolution (≤10 kyr) oxygen isotope records (Zachos et al., 2001b; Wade and Pälike, 2004; Pälike et al., 2006a,b; Billups et al., 2002).

Published by Copernicus Publications on behalf of the European Geosciences Union.

In 2003, the Ocean Drilling Program (ODP) revisited Walvis Ridge (29° S) in the southeastern Atlantic Ocean during Leg 208 (Zachos et al., 2004). Six sites were drilled along a depth-transect of which two sites, Site 1264 (2505 m) and Site 1265 (3083 m), are used in this study to assess the long-term orbital pacing theory of the early Miocene time interval. Both sites are situated above the level of the present day lysocline and CCD (Fig. 1). This offers the unique opportunity to record major changes in regional and/or global ocean carbon chemistry, ocean circulation and intermediate bottom water chemistry and circulation during key paleoceanographic events (Zachos et al., 2004). Site 1264 was drilled as the shallow water depth end-member of the Walvis Ridge transect and is characterized by an expanded Oligocene and Neogene sediment sequence (Zachos et al., 2004). From this site, we have generated a high-resolution (<3 kyr) and continuous stable isotope record of the benthic foraminiferal species *Cibicidoides mundulus* between ∼24–19 Ma. In this paper, we will compare our new isotope results with those of ODP Site 926 Hole B (3° N) at 3598 m water depth and ODP Site 929 Hole A (6° N) at 4358 m water depth, both from Ceara Rise in the Equatorial Western Atlantic (Flower et al., 1997a, Zachos et al., 1997, 2001b; Paul et al., 2000; Pälike et al., 2006a; Shackleton et al., 2000), and the composite record of ODP Site 1090, based on Holes D and E, at 3699 m water depth from the Agulhas Ridge (43° S) in the Atlantic section of the Southern Ocean (Billups et al., 2002, 2004). In addition, we decompose the marine benthic δ^{18}O record into temperature and ice volume contributions through an inverse modeling technique (De Boer et al., 2010; Bintanja and Van de Wal, 2008), in order to shed new light upon the orbital pacing theory of the Antarctic ice sheets during the Oligocene/Miocene transition.

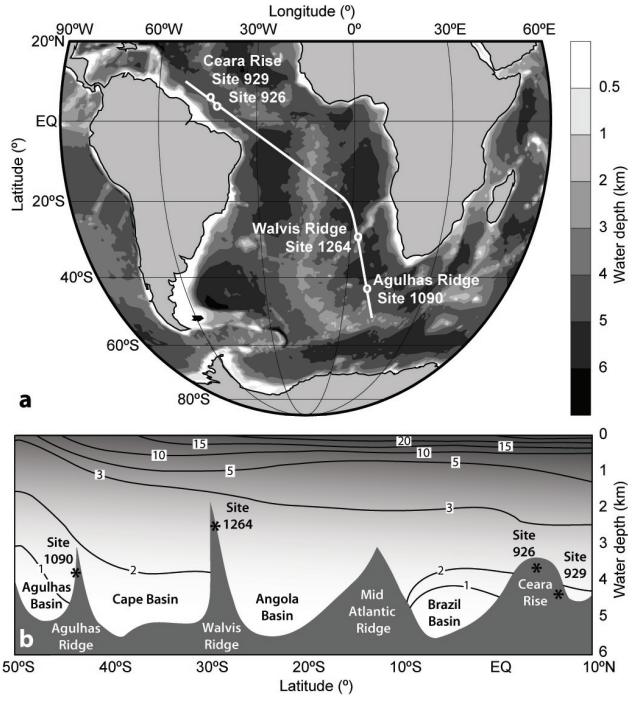

Fig. 1. Site locations and Atlantic Ocean transect. **(a)** Present day map of the drill locations of ODP Sites 929, 926, 1264 and 1090. The white line through the drill locations represents the approximate transect shown in panel (b). **(b)** Transect through the current Equatorial and Southern Atlantic Ocean. Black stars represent drill locations. Black lines represent present-day water temperatures. Both graphs were constructed using Ocean Data View (Schlitzer, 2010) and were then graphically edited.

2 Analytical methods

Samples of approximately 10 g of sediment were taken every 2–2.5 cm from the latest Oligocene and early Miocene part of the Site 1264. The samples were freeze dried, washed (in tap water), sieved to obtain the larger than 37, 65 and 150 µm fractions for foraminiferal accumulation rates (not presented in this study) and foraminiferal analysis, and dried in evaporation basins. Primarily single specimen samples of the benthic foraminifer species *Cibicidoides mundulus* were picked from the >150 µm fraction and subsequently analysed. For every sample, stable oxygen and carbon isotope ratios (δ^{18}O and δ^{13}C, respectively) were measured and the δ^{18}O values were corrected for disequilibrium with seawater by adding 0.64 ‰ (Shackleton, 1974; Zachos et al., 2001a).

Approximately 80 % of the samples were measured at the Faculty of Geosciences of Utrecht University (UU) where (uncleaned) foraminiferal tests were dissolved in a Finnigan MAT Kiel III automated preparation system. Isotopic ratios of purified CO_2 gas were then measured on-line with a Finnigan MAT 253 mass spectrometer and compared to an internal gas standard. The remaining part was measured at the Department of Geological Sciences of the University of Florida (UF) on two intercalibrated devices. Of the samples with sufficient specimens, subsamples of crushed, washed (in hydrogen peroxide) and ultra-sonically cleaned (in methanol) foraminiferal calcite from several tests (3–6 on average) was reacted using a common acid bath of orthophosphoric acid at 90 °C using a Micromass Isocarb preparation system. Isotope ratios of purified CO_2 gas were measured online using a Micromass Prism mass spectrometer. Of the samples with few *Cibicidoides mundulus* specimens, whole, washed (in hydrogen peroxide) and ultra-sonically cleaned (in methanol) foraminiferal test(s) (1–2 specimen) were dissolved using a Finnigan MAT Kiel III automated preparation system coupled to a Finnigan MAT 252 mass spectrometer to measure the isotopic ratios of purified CO_2 gas. The standard NBS-19 and the in-house (at UU) standard "Naxos" were used to calibrate to Vienna Pee Dee Belemnite (VPDB). Reproducibility (same sample on the same device) is 0.19 ‰ for δ^{18}O and 0.13 ‰ for δ^{13}C (Supplement Fig. 1).

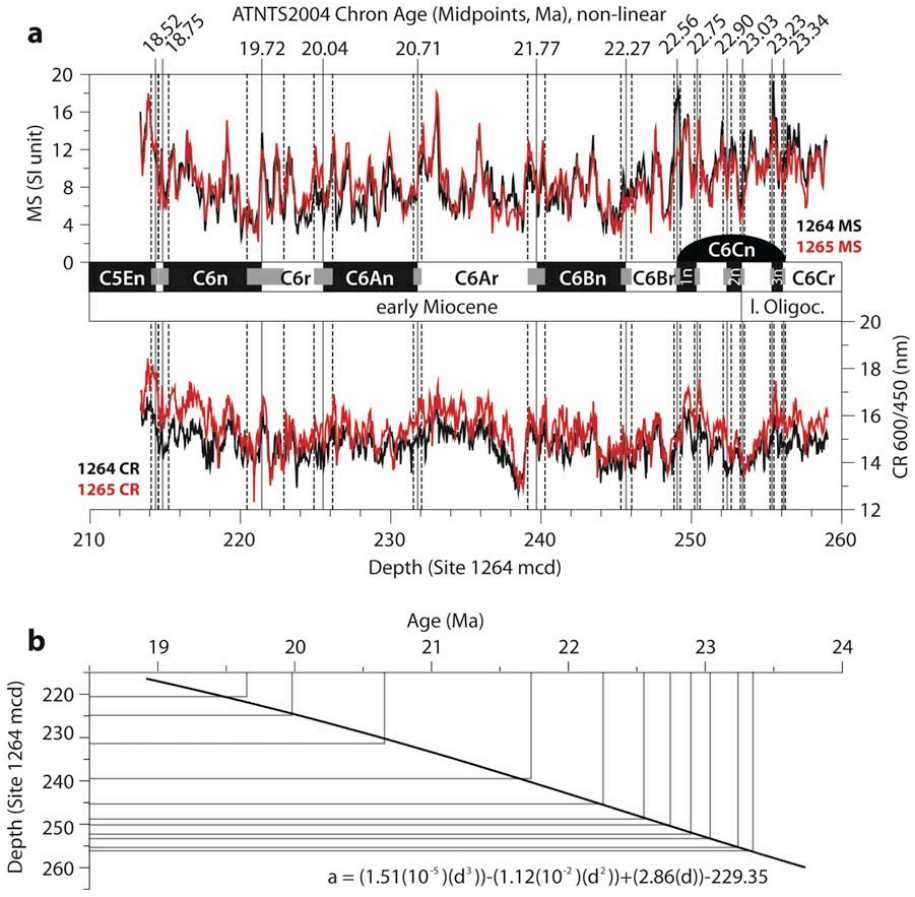

Fig. 2. Age model. **(a)** Transfer of the magnetostratigraphy (Bowles, 2006) from Site 1265 to Site 1264 by means of magnetic susceptibility (MS) and 600/450 nm colour reflectance (CR) pattern matching. Depth scale is in meters composite depth (mcd). Please note: by transferring the magnetostratigraphic mid-points from Site 1265 mcd to Site 1264 mcd, they may not look like "mid-points" on Site 1264 mcd. **(b)** 3rd order polynomial fit of depth "*d*" through ATNTS2004 (Lourens et al., 2004) chron ages "*a*".

An average offset of ∼0.30 ‰ in δ^{18}O is found between the analyses of foraminifera from the same samples by the two labs (Supplement Fig. 1). No correction has been applied for this offset because a lower resolution record (step size ∼100 kyr), spanning the interval of this study and measured entirely at UF, shows no offset with the UU measurements (B. D. A. Naafs, unpublished data). Furthermore, the relatively small set of samples used to compare the isotope signatures between laboratories might not be representative. Only 20 outliers were defined by an upper and lower boundary of 2 standard deviations (of the entire time series) added or subtracted from a 13-point moving average. Because the stable isotope analysis is paired, outliers defined in δ^{13}C or in δ^{18}O were removed from both records (Supplement Fig. 2). Where possible, outliers were re-measured. After outlier-removal, the stable isotope records of Site 1264 contain 1754 data points.

3 Age model

Because Site 1264 lacks a good magnetostratigraphy, we transferred the magnetostratigraphic data (Bowles, 2006) from the nearby ODP Site 1265 by pattern matching the magnetic susceptibility (MS) and colour reflectance (CR, 600/450 nm) records (Fig. 2, Table 1). Subsequently, we assigned the Astronomically Tuned Neogene Time Scale 2004 (ATNTS2004) ages of Lourens et al. (2004) to the magnetic reversals and applied a third order polynomial to inter- and extrapolate the age model. This resulted in an orbital-based age model without tuning individual peaks to the astronomical solution. We chose to present our data on an un-tuned, but loosely astronomy-based, timescale to re-examine previous interpretations about the Oligocene and Miocene climate dynamics. Finally, the "Match" algorithm (Lisiecki and Lisiecki, 2002) was applied to correlate the stable isotope records of Ceara Rise and the Agulhas Ridge to Site 1264.

Table 1. Chron ages.

Chron	Site 1265 Mid-point depth (mcd)[a]	Site 1264 Mid-point depth (mcd)[b]	ATNTS-2004 age (Ma)[c]	3rd order polynomial age (Ma)[d]
C5En (o)	89.745	214.408	18.524	18.564
C6n (y)	90.395	214.878	18.748	18.644
C6n (o)	97.095	221.450	19.722	19.592
C6An (y)	100.420	225.520	20.040	20.102
C6An (o)	105.595	231.792	20.709	20.826
C6Bn (y)	112.720	239.685	21.767	21.662
C6Bn (o)	118.595	245.615	22.268	22.261
C6Cn.1n (y)	121.500	248.937	22.564	22.593
C6Cn.1n (o)	122.390	250.333	22.754	22.733
C6Cn.2n (y)	124.110	252.323	22.902	22.934
C6Cn.2n (o)	124.815	253.342	23.030	23.037
C6Cn.3n (y)	126.145	255.298	23.230	23.237
C6Cn.3n (o)	126.740	256.070	23.340	23.317

[a] Midpoints between the top and bottom uncertainties in magnetic reversals (Bowles, 2006). Depth scale is in meters composite depth (mcd).

[b] Based on calibration shown in Fig. 2.

[c] Astronomically Tuned Neogene Time Scale (Lourens et al., 2004).

[d] 3rd order polynomial based on the ATNTS2004 (Lourens et al., 2004) graphed in Fig. 2.

4 Stable isotope results

The δ^{18}O record of Site 1264 matches that of the Agulhas Ridge Site 1090 very well (Figs. 3 and 4). Both records are, however, ∼0.5 ‰ heavier than the δ^{18}O records of Sites 926 and 929. These distinct δ^{18}O (and δ^{13}C) gradients between sites disappeared, however, during two "events" at ∼22.9 Ma and ∼21.2 Ma, which are marked by low $\Delta\delta^{18}$O values (Fig. 4). Especially the δ^{18}O values at Site 929 increased significantly during these events. Changes in wind-driven (Cramer et al., 2009), thermal and/or haline ocean circulation and in ocean gateway configurations (Von der Heydt and Dijkstra, 2006) have been proposed to explain changing inter- and intrabasinal isotope gradients. We interpret these events as periods where at the Ceara Rise abyss, an Antarctic sourced bottom-water mass was present (Woodruff and Savin, 1989; Billups et al., 2002) and hence as periods in which the prevailing mechanism that kept the gradients in place, was briefly (<400 kyr) disrupted. The ∼0.4 ‰ difference in the average δ^{18}O values before and after the O/M transition at Ceara Rise (Zachos et al., 2001b) is not recorded at Site 1264, suggesting that a possible flow reversal through the Panamanian Seaway (Von der Heydt and Dijkstra, 2006) or changes in abyssal circulation patterns in the Atlantic (Miller and Fairbanks, 1983) did not significantly alter the δ^{18}O composition of the water mass at Site 1264.

The carbon isotope record of Site 1264 is on average 0.1 to 0.4 ‰ heavier than those of Sites 1090, 926 and 929, indicating that Site 1264 bathed in relatively nutrient-depleted intermediate water masses due to its shallower position (Figs. 1, 3 and 4). The highest δ^{13}C value of almost 2.0 ‰ coincides with the onset of the Oligocene-Miocene Carbon Maximum, CM-OM (Hodell and Woodruff, 1994), and corresponds (Zachos et al., 1997) with the maximum δ^{18}O values during the O/M climate transition. The sudden decline in δ^{13}C values of ∼0.4 ‰, marking the end of the CM-OM around ∼21.8 Ma, coincides with a significant change in the deep-sea carbon reservoir within the entire Atlantic Ocean (Figs. 3 and 4).

Power spectral analyses indicate the dominance of the long-term (400 kyr) eccentricity cycle in both the δ^{13}C and δ^{18}O records (Fig. 5). Additional smaller peaks are found at the short (95 and 125 kyr) eccentricity periods and to a lesser degree at the obliquity (41 kyr) period. No clear precession-related peaks are detected in the power spectra even though the resolution of the record (<3 kyr) is well above the Nyquist limit for this cycle. The weak imprint of obliquity at Site 1264 is remarkable, since Sites 926 and 929 revealed a dominant obliquity signal at these times (e.g. Paul et al., 2000; Flower et al., 1997b). The stronger obliquity signal at the tropical deep-water Sites 929 and 926, and the weaker imprint recorded at the high(er) latitude intermediate- to deep-water Sites 1264 and 1090 is still open for speculation about possible deep-water sources and teleconnections between the poles and the equator.

Wavelet analysis confirms the dominance of the 400 kyr eccentricity-related variability in the δ^{13}C and δ^{18}O records throughout the time interval studied (Fig. 5, Supplement Fig. 3). The ∼100 kyr eccentricity-related variations in δ^{18}O occur during four distinct and two less distinct periods. These periods are also reflected in the wavelet spectrum of δ^{13}C, although the relative amplitude of the ∼100 kyr dominated intervals differs slightly from that of the δ^{18}O record (Fig. 5). Sites 1090, 929 and 926 do not show these prominent ∼100 kyr dominated intervals. Since these sites are situated approximately 1–1.5 km deeper than Site 1264, we consider that they were more vulnerable to carbonate dissolution through changes in the position of the CCD and lysocline.

5 Inverse modelling

A set of 1-D ice sheet models for West and East Antarctica, Greenland, North America and Eurasia in combination with an inverse routine was applied to separate the δ^{18}O signal into a temperature (δ_T) and an ice volume (δ_w) component (De Boer et al., 2010, 2011). The model was initially designed to unravel ice-volume and temperature components from a global benthic δ^{18}O stack (Bintanja et al., 2005; De Boer et al., 2010), which is anchored in the present day (PD). Since we have applied this method to Site 1264 only, we assumed that the average δ^{18}O value approximates that of the global mean bottom-water for the early Miocene, notwithstanding a mean offset of 0.53 ‰ to heavier values with respect to the global stack of Zachos et al. (2001a, 2008). All calculations are based relative to a PD δ^{18}O value of 3.23 ‰ (Zachos et al., 2008). Previously performed

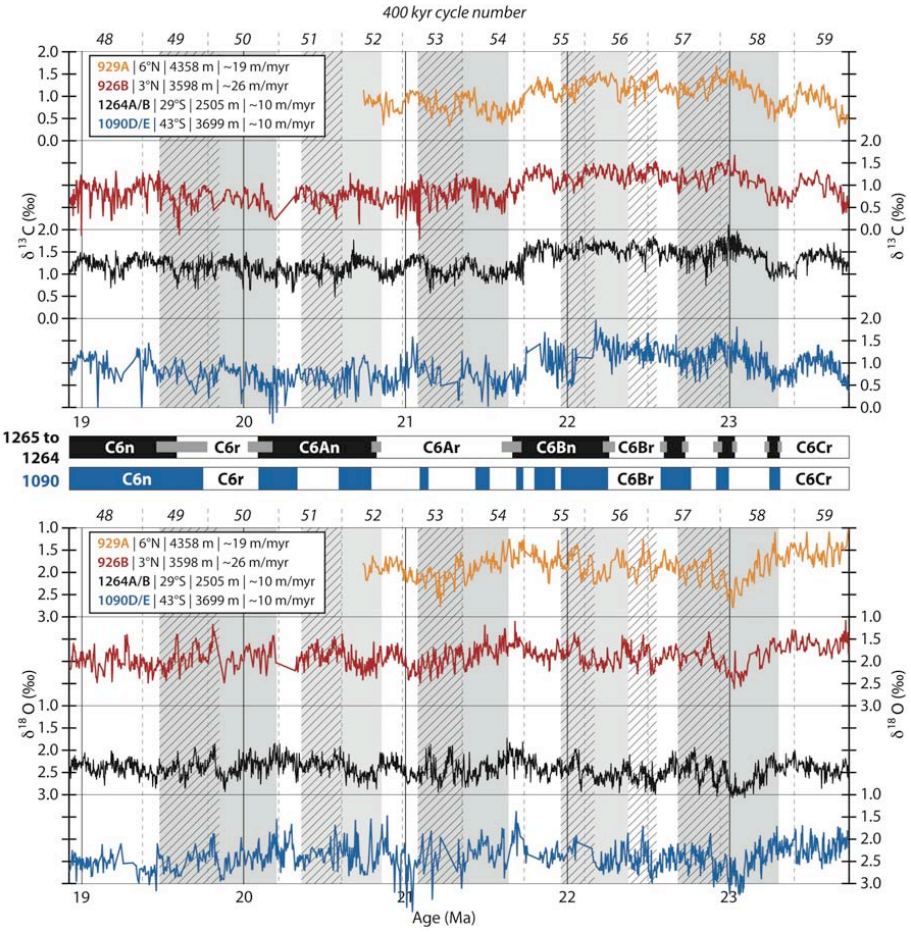

Fig. 3. Comparison of early Miocene stable isotope records. High-resolution Atlantic δ^{13}C and δ^{18}O (+0.64 ‰) records of ODP Sites 929, 926 (Flower et al., 1997a; Zachos et al., 1997, 2001b; Paul et al., 2000; Pälike et al., 2006a; Shackleton et al., 2000), Site 1264 (this study) and Site 1090 (Billups et al., 2002, 2004). Records were matched to Site 1264 in the depth domain using the "Match" algorithm (Lisiecki and Lisiecki, 2002) and then plotted on the ATNTS-based age model of Site 1264. The Walvis Ridge magnetostratigraphy (Bowles, 2006) has been transferred from Site 1265 to Site 1264 (see Fig. 2). The vertical dashed lines mark the boundaries of the 400 kyr cycles (Wade and Pälike, 2004). Latitude, present water depth and average sedimentation rates are given for each site.

sensitivity tests revealed that the error margin around absolute modeled values is of the order of 10 %. For a thorough evaluation of the set of 1-D models utilized in this study we refer to De Boer et al. (2011).

The modeled δ_T record is assumed to represent a global value for deep-water temperature (ΔT_{dw}) relative to the present day, and was rescaled into continental mean annual Northern Hemisphere (40–80° N) air temperature (ΔT_{NH}) using a simple linear equation (Bintanja et al., 2005). The ice-volume component (δ_w) can be expressed in the amount of sea level change, which is equivalent to the amount of land-ice storage on Antarctica and the Northern Hemisphere (mainly Greenland). For the 400 and ~100 kyr oscillations we find within the uncertainty band of the cross spectral analyses, an in-phase relation between δ_T and δ_w, which implies that polar cooling and ice-sheet growth occurred (almost) simultaneously (Fig. 6). This is in agreement with the model reconstructions of the late Pleistocene ~100 kyr glacial-interglacial rhythm that showed similar in-phase behaviour for the terminations and a small lag of global ice volume to air temperature of ~6 kyr for the glacial inceptions (Bintanja and Van de Wal, 2008).

The outcome of our ice-sheet model simulations show that changes in δ^{18}O are accompanied by large shifts in ΔT_{NH} of up to 10–15 °C (Fig. 6, Supplement Fig. 4). The main sea level changes are linked to ice-sheet fluctuations on Antarctica. A change from half to full present-day Antarctic ice-sheet configuration is estimated for Mi-1 at 23 million years ago. At this time, the combined West and East Antarctic ice sheets had reached their maximum size of the time interval studied, resulting in a global sea level of ~2.5 m above present-day, indicating that the Antarctic ice sheet had reached (almost) its present-day size. These findings are in agreement with estimated apparent sea level variations

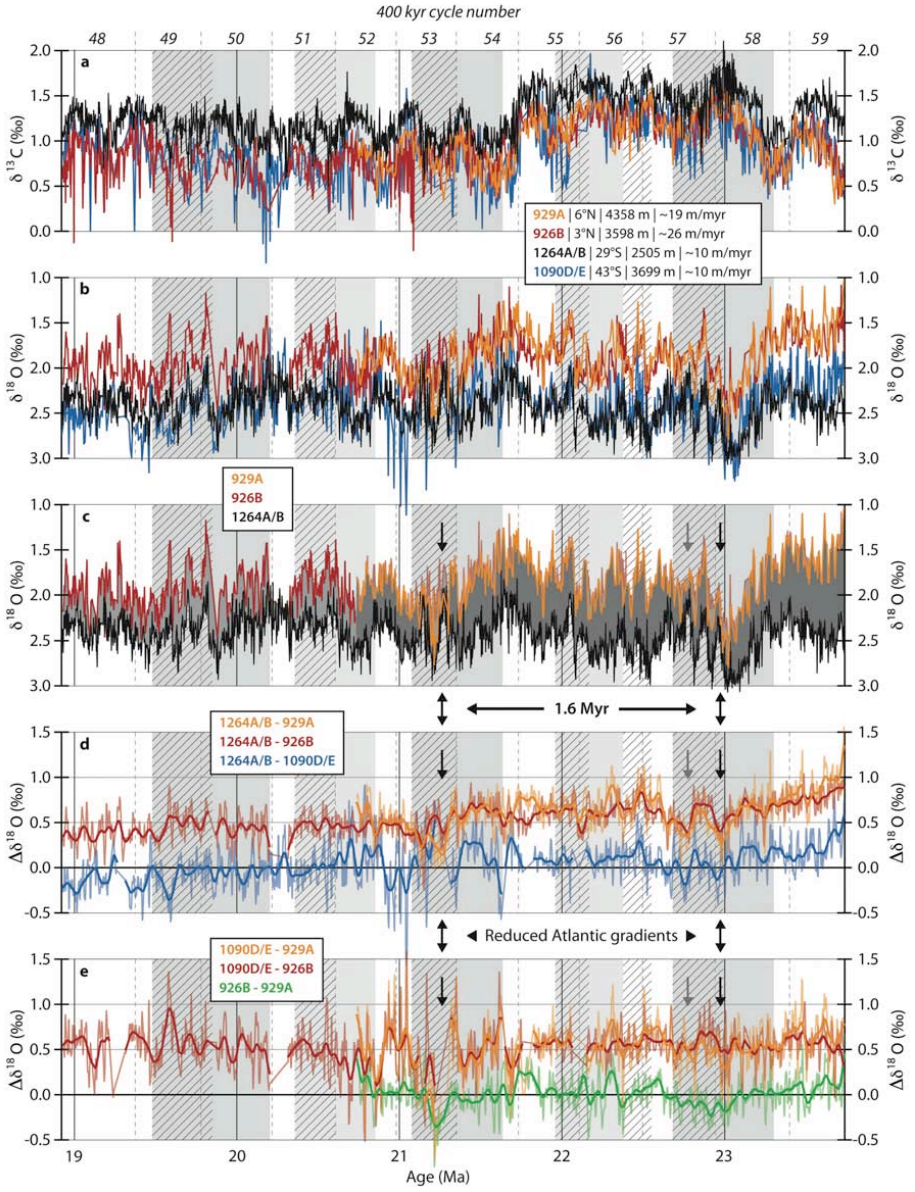

Fig. 4. Comparison of early Miocene stable isotope records. For more information see figure caption of Fig. 3. **(a)** The δ^{13}C records. **(b)** The δ^{18}O (+0.64 ‰) records. **(c)** As in panel (b). but without Site 1090. Gray areas in between the isotope records indicate the changes in Atlantic (intermediate) deep-water δ^{18}O gradients. **(d)** $\Delta\delta^{18}$O of Sites 1264 – 929, 1264 – 926, and 1264 – 1090, to indicate the changes in Atlantic (intermediate) deep-water δ^{18}O gradients. Shaded lines represent the $\Delta\delta^{18}$O of the 2 kyr resampled data sets. Resampling was done using a Gaussian-weighted moving average (15 kyr). Thick lines are the corresponding 100 kyr Gaussian-weighted moving averages. Arrows indicate the occurrences of reduced gradients between equatorial and southern Atlantic. These two events occur 4×400 kyr apart. **(e)** As in panel (d) but now for 1090 – 929, 1090 – 926 and 926 – 929.

related to the East Antarctic ice sheet (Pekar and DeConto, 2006), which indicate changes of similar amplitude. Although there is a very small amount of Greenland ice volume modelled, this is probably not significant considering the uncertainty of the global mean δ^{18}O value during this interval (De Boer et al., 2011).

Wavelet analyses of the sea level and temperature components of δ^{18}O revealed an almost similar pattern as the δ^{18}O record. The episodes of ∼100 kyr dominated δ^{18}O variability, and resultant ∼100 kyr dominated ice volume and ΔT_{NH}, are preceded by an interval of gradual cooling and glacial build-up. In fact, the ∼100 kyr dominated episodes seem to coincide with the termination phase of periods of large Antarctic ice sheet expansion (Fig. 6). Following the astronomical naming scheme based on the 400 kyr cycle of Earth's eccentricity (Wade and Pälike, 2004), the oldest recorded Antarctic ice sheet expansion (Mi-1) starts within cycle 58 at ∼23.4 Ma and ends within cycle 57 at

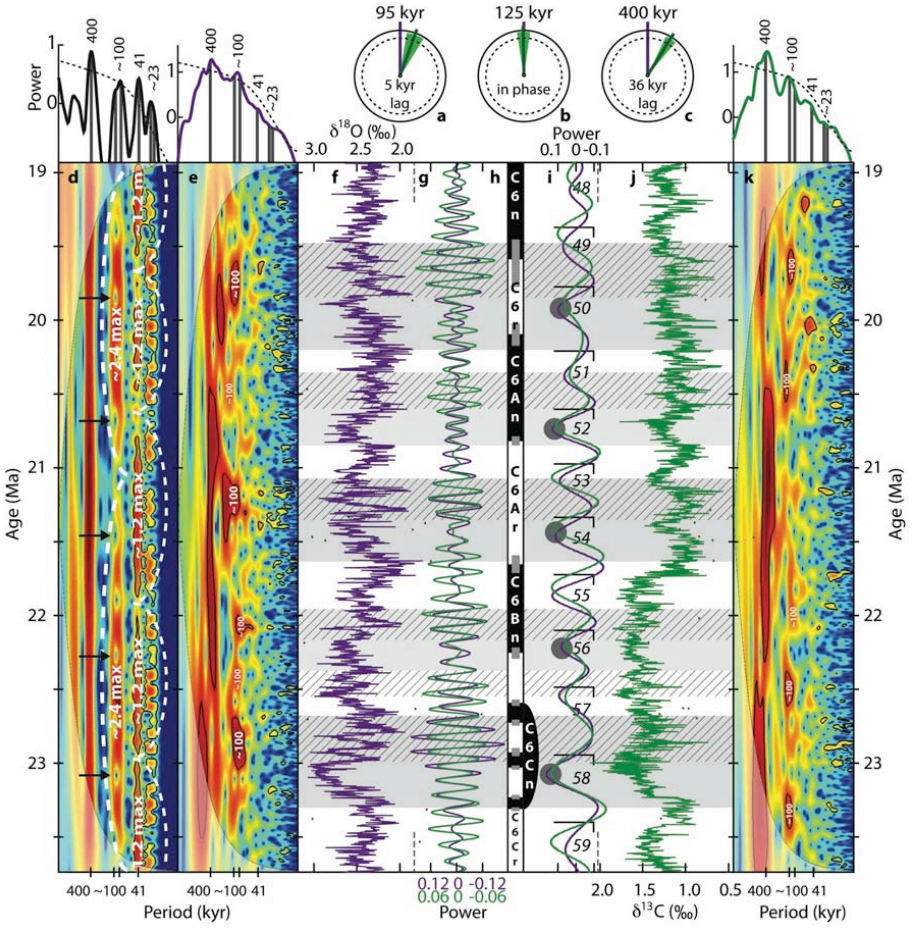

Fig. 5. Walvis Ridge (Site 1264) stable isotope records. Phase wheels represent the phase relation between δ^{18}O (purple) and δ^{13}C (green) at the **(a)** 95, **(b)** 125 and **(c)** 400 kyr eccentricity periods, where 360° represents one full cycle. Phase lags increase clockwise and the green areas represent the 95 % confidence level. Vector length shows coherency (dashed circle 95 %). **(d)** Wavelet analysis (Grinsted et al., 2004) with >95 % confidence levels (black lines) of an eccentricity/obliquity/precession mix calculated after the Laskar et al. (2004) astronomical solution. Time step size after re-sampling is 2.75 kyr. White dashed lines indicate the (on average) ∼1.2 and ∼2.4 Myr amplitude modulation of obliquity and eccentricity. Arrows indicate minima in 400 kyr eccentricity (characterized by a smaller amplitude 100 kyr cycle) that coincide with maximum ice-sheet expansion. These minima are timed 1×, 2× or 4 × 400 kyr apart. On top the global spectrum (Torrence and Compo, 1998) with >95 % confidence level. **(e)** Wavelet analysis and global spectrum – processed as in panel (d) – of δ^{18}O record after removal of >0.5 Myr periodicities using a notch filter (Paillard et al., 1996) (f: 0.0, bw: 2.0) and normalization. **(f)** Oxygen isotope (δ^{18}O + 0.64 ‰) record from Site 1264. Loose dots represent outliers. **(g)** Gaussian filters (Paillard et al., 1996) (∼100 kyr, f: 10.0, bw: 2.0) of the δ^{18}O (purple) and δ^{13}C (green) records. **(h)** Transferred magnetostratigraphy (Bowles, 2006) from Site 1265 to Site 1264. Black is normal, white is reversed, gray is uncertain. **(i)** Gaussian filters (Paillard et al., 1996) (400 kyr, f: 2.5, bw: 1.0) of the δ^{18}O (purple) and δ^{13}C (green) records, with corresponding 400 kyr cycle numbers (Wade and Pälike, 2004). Gray circles mark maxima of the ice-sheet expansion phases. **(j)** Carbon isotope (δ^{13}C) record from Site 1264. Loose dots represent outliers. **(k)** Wavelet analysis and global spectrum of δ^{13}C – processed as in panel (d).

∼22.6 Ma (Figs. 6 and 7). Similar patterns are reflected by the ice-sheet expansion phases at 22.3–21.9 Ma (cycles 56–55), 21.6–21.1 Ma (cycles 54–53), and 20.2–19.4 Ma (cycles 50–49) of which the latter two periods are close within the age estimates of the Mi-1a and Mi-1aa episodes (Wright and Miller, 1992), respectively (Fig. 8).

6 Discussion

Cross spectral analysis between the δ^{18}O and δ^{13}C records reveals that both records are highly coherent at the eccentricity periodicities with the δ^{13}C record slightly lagging δ^{18}O by 36 ± 8, 0 ± 3 and 5 ± 3 kyr for the 400, 125 and 95 kyr periods, respectively (Fig. 5). Almost similar results were found for the δ^{13}C and δ^{18}O records of Ceara Rise and the Pacific Site 1218 for the Oligocene time interval, indicating

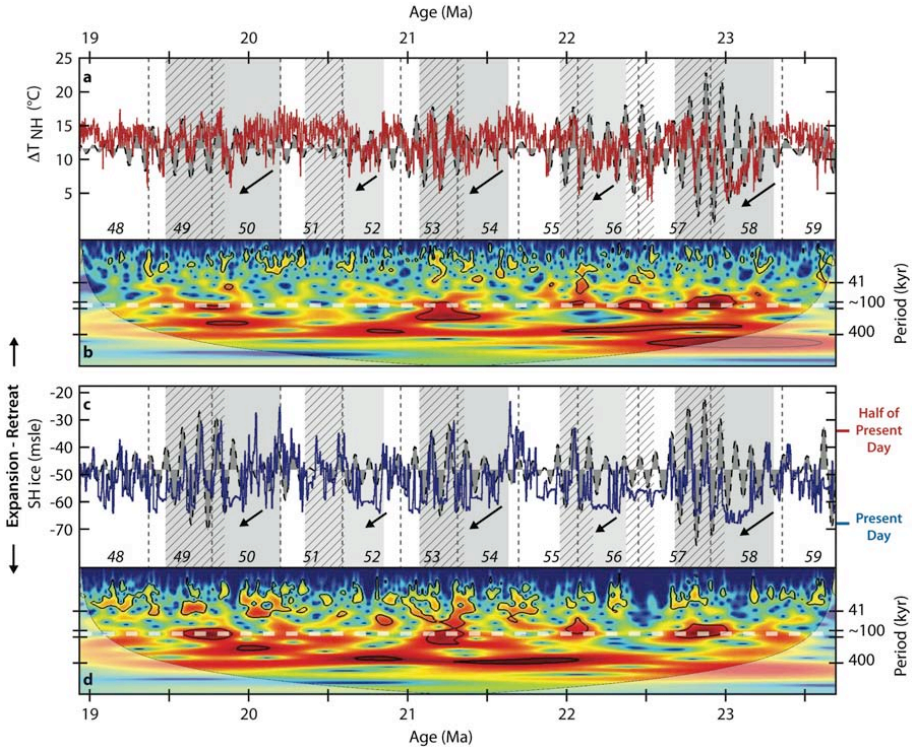

Fig. 6. 1-D inverse modelling output (De Boer et al., 2010). **(a)** Northern Hemisphere (40–80° latitude) annual average air temperature, with ∼100 kyr filtered component (f: 10.0, bw: 2.0) (Paillard et al., 1996) depicted in the background. **(b)** Wavelet analysis (Grinsted et al., 2004) of NH temperature variability. Data processed as in Fig. 5. **(c)** Antarctic ice, with ∼100 kyr filtered component (f: 10.0, bw: 2.0) (Paillard et al., 1996) depicted in the background. **(d)** Wavelet analysis (Grinsted et al., 2004) of Southern Hemisphere (Antarctic) ice variability (in meter sea level equivalent). Data processed as in Fig. 5. White dashed lines indicate the ∼100 kyr period. Vertical dashed lines and numbers in italic represent the 400 kyr cycle numbers (Wade and Pälike, 2004).

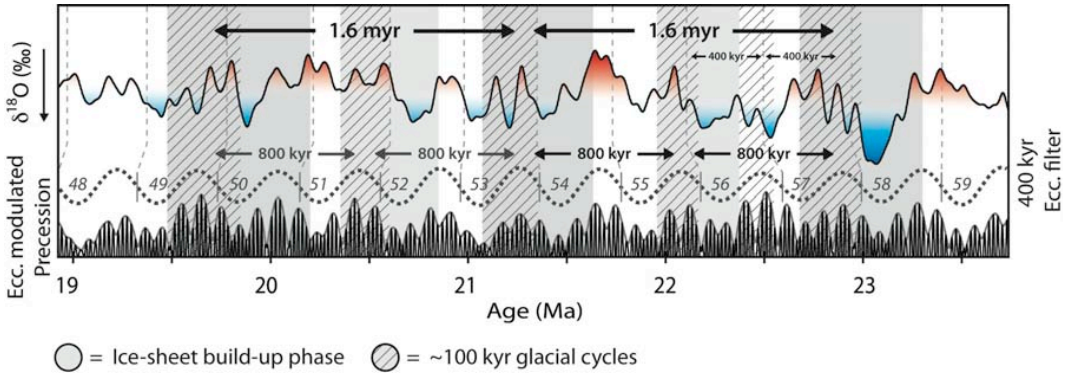

Fig. 7. Pacing of ∼100 kyr dominated glacial cycles. At the top a Gaussian-weighted moving average (100 kyr) of Site 1264 δ^{18}O record is depicted. The bottom graphs represent eccentricity modulation precession, eccentricity (Laskar et al., 2004) and a 400 kyr filter (f: 2.5, bw: 1.0) of eccentricity. The 400 kyr numbers of Wade and Pälike (2004) are shown on top of the 400 kyr eccentricity filter. Because the δ^{18}O record of Site 1264 is presented on an un-tuned age model, our 400 kyr cycle marking is tentative and no conclusions should be drawn based on the phase relation with eccentricity as depicted. For Figs. 3–8: gray areas indicate cooling periods with reduced ∼100 kyr power, gray and striped areas indicate ∼100 kyr "worlds", white areas are intermediate phases characterized by a greater non-linear response to eccentricity modulated precession. These ∼100 kyr dominated episodes occur 1 ×, 2 × and 4 × 400 kyr apart from each other. The Oligocene – Miocene transition shows up as one of four/five "similar" episodes. It stands apart mainly by the duration of the glaciation phase. Almost comparable absolute high δ^{18}O values are reached during the other glacial episodes as well, but they last too short to be picked up by the moving average.

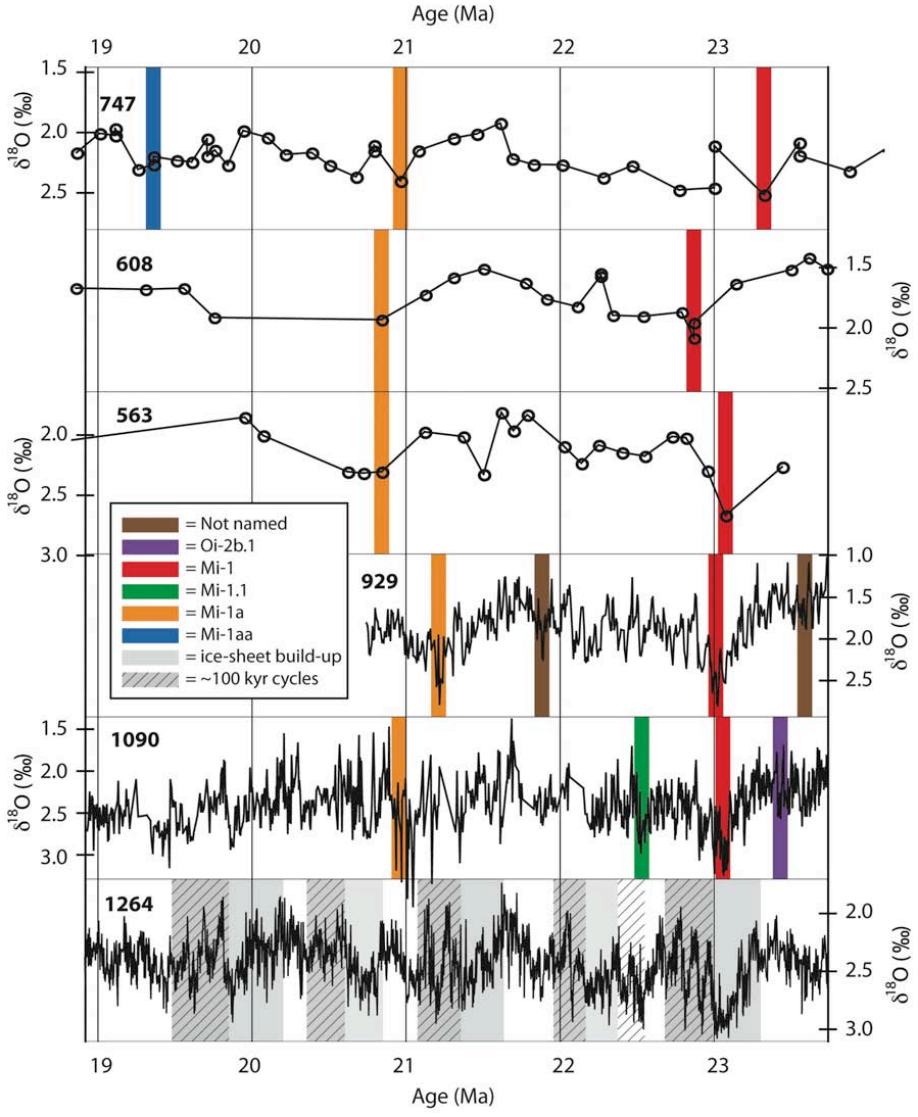

Fig. 8. Transcription of latest Oligocene and early Miocene Oi- and Mi-naming scheme through time. Comparison between isotope records from the Kerguelen Plateau Site 747 and the North Atlantic Sites 563 and 608 (Wright et al., 1992; Wright and Miller, 1992) with Site 1264 (this study). Ages of Sites 563, 608 (Berggren et al., 1995) and magnetostratigraphy of Site 747 (Oslick et al., 1994) have been recalculated to the ATNTS2004 (Lourens et al., 2004). Site 929 (Zachos et al., 1997, 2001b; Paul et al., 2000) and Site 1090 (Billups et al., 2002, 2004) are plotted on the Walvis Ridge Site 1264 age model. The Oi- and Mi-zones or episodes were first described at Sites 563, 608 and 747. These names were then (sometimes erroneously) transposed to Sites 929 and 1090. The ∼100 kyr dominated intervals described in this study shed new light on the major zones/episodes in the early Miocene and are close within the age estimates of the previously described Mi-1, Mi-1a and Mi-1aa zones or episodes. Nevertheless we support a 400 kyr number-based naming scheme (e.g. Wade and Pälike, 2004).

a strong coupling between climate states and changes in the oceanic carbon reservoir (Zachos et al., 1997, 2001b; Paul et al., 2000; Pälike et al., 2006b). Since insolation changes operate predominantly on precession and obliquity time scales, a non-linear mechanism should be involved to transfer power from these high-frequency astronomical periods to the eccentricity band. Using simple box model experiments, Pälike et al. (2006b) showed that the seasonal insolation cycle can drive changes in biosphere productivity and carbon burial on eccentricity time scales due to the long residence time of carbon in the ocean. During periods of increased carbon burial (e.g. high $\delta^{13}C$ values), atmospheric pCO_2 concentrations will drawdown, thereby setting the stage for global cooling and ice-sheet expansion. In turn, during glacial phases the meridional temperature gradient should be stronger, which may have led to enhanced upwelling intensities and carbon burial (Zachos et al., 2001b). A lowering of the sea level may also have enhanced productivity conditions due to erosion of

the continental shelves. Evidence for an increase in productivity during the Oligocene/Miocene transition was inferred from benthic foraminifer accumulation rates (Diester-Haass et al., 2011). These changes in marine primary productivity are found to be in phase with long- and short-term eccentricity. Thus, insolation-forced changes in the carbon cycle may act as an important modulator for global climate change on eccentricity time scales during the early Miocene as was found for the Oligocene (Pälike et al., 2006b).

The major large-scale Antarctic ice-sheet expansions coincide with 400 kyr eccentricity minima when the power of the ∼100 kyr eccentricity cycle is significantly suppressed (e.g. at ∼23.1, ∼22.3, ∼21.4, and ∼19.8 Ma, black arrows in Fig. 5). Since these major ice-sheet expansions do not occur at every 400 kyr eccentricity minimum, one might expect that they are modulated by the long-term eccentricity and obliquity components (e.g. Lourens and Hilgen, 1997; Zachos et al., 2001b; Billups et al., 2002; Pälike et al., 2006a,b). In particular, reduced amplitude of the tilt cycle over hundred thousands of years in combination with low eccentricity values may have favoured Antarctic ice sheet build-up due to on average low summer insolation values (Zachos et al., 2001b). Except for Mi-1, the link between the long-term (∼1.2 Myr) obliquity and the (∼2.4 Myr) eccentricity modulation and the ice-sheet expansion phases are as yet too inconsistent to suggest a strong causal relationship between them (Fig. 5). This suggests that another non-linear mechanism of some kind should have been involved. An example of a non-linear mechanism could be that a threshold size for a stable Antarctic ice sheet had been passed, which triggered an episode with large scale deglaciations every ∼100 kyr. During these periods, the ice sheets were probably not adequately shaped (e.g. DeConto and Pollard, 2003) to enter a new major growth episode at the next minimum of the 400 kyr cycle.

In summary, long-term tectonic or oceanographic processes may have preconditioned atmospheric pCO_2 levels through changes in the carbon cycle to set the stage for dominantly eccentricity-paced episodes of large Antarctic ice-sheet expansions during the late Oligocene and early Miocene. Such a hypothesis would be in line with modelling studies (DeConto et al., 2008) and reconstructed atmospheric pCO_2 levels for this time interval (Kürschner et al., 2008; Pagani et al., 1999). The termination phases of these episodes are characterized by enhanced climate variability on ∼100 kyr (short eccentricity) time scales. During at least two of these termination-phases, bottom to intermediate water $\delta^{18}O$ gradients in the Atlantic ceased to exist, indicating a direct link between global climate, enhanced ice sheet instability and major oceanographic reorganisations. This succession of global changes could have triggered the major species turnover events as found on the continents during the early Miocene (Van Dam et al., 2006).

Supplementary material related to this article is available online at: http://www.clim-past.net/7/869/2011/cp-7-869-2011-supplement.pdf.

Acknowledgements. We are indebted to Geert Ittman, Arnold van Dijk, Jan Drenth, Jason Curtis, Giana Brown, Walter Hale, Gert-Jan Reichart, and Klaudia Kuiper for their (technical) assistance. David Naafs, Martin Ziegler, Steven Bohaty, Clara Bolton, Lucy Stap, Tanja Kouwenhoven, Sietske Batenburg, Christian Zeeden, Helen Beddow-Twigg, Cristina Sghibartz, Sarah O'Dea, Rosanna Greenop, Frits Hilgen, Ellen Thomas, Dick Kroon, Paul Wilson, Gavin Foster and Eelco Rohling are thanked for discussing the science and/or commenting on an earlier version of this manuscript. We would like to thank the anonymous referee and Franck Bassinot for their insightful comments. Luc Beaufort is thanked for editing the manuscript. This research used samples provided by the Ocean Drilling Program, sponsored by the US National Science Foundation and participating countries under the management of Joint Oceanographic Institutions (JOI), Inc. This study has been made possible by NWO VIDI-grant no. [864.02.007] and VICI-grant no. [865.10.001] assigned to L. J. L. and the European Community's Seventh Framework Programme (FP7/2007-2013) under grant agreement no. [215458] to the GTS-next project (D. L. and H. P.).

Edited by: L. Beaufort

References

Beaufort, L.: Climatic importance of the modulation of the 100 kyr cycle inferred from 16 myr long Miocene records, Paleoceanography, 9, 821–834, 1994.

Berggren, W. A., Kent, D. V., Swisher, C. C., and Aubry, M.-P.: A Revised Cenozoic Geochronology and Chronostratigraphy, in: Geochronology, time scales and global correlation, edited by: Berggren, W. A., Kent, D. V., Aubry, M.-P., and Hardenbol, J., 54, 129–212, 1995.

Billups, K., Channell, J. E. T., and Zachos, J.: Late Oligocene to early Miocene geochronology and paleoceanography from the subantarctic South Atlantic, Paleoceanography, 17(1), 1004, doi:10.1029/2000PA000568, 2002.

Billups, K., Pälike, H., Channell, J. E. T., Zachos, J., and Shackleton, N. J.: Astronomic calibration of the late Oligocene through early Miocene geomagnetic polarity time scale, Earth Planet. Sc. Lett., 224, 33–44, 2004.

Bintanja, R. and Van de Wal, R. S. W.: North American ice-sheet dynamics and the onset of 100 000-year glacial cycles, Nature, 454, 869–872, 2008.

Bintanja, R., Van de Wal, R. S. W., and Oerlemans, J.: Modelled atmospheric temperatures and global sea levels over the past million years, Nature, 437, 125–128, 2005.

Bowles, J.: Data report: revised magnetostratigraphy and magnetic mineralogy of sediments from Walvis Ridge, Leg 208, in: Proc. ODP, Sci. Results, 208: College Station, TX (Ocean Drilling Program), edited by: Kroon, D., Zachos, J. C., and Richter, C., 1–24, doi:10.2973/odp.proc.sr.208.206.2006, 2006.

Cramer, B. S., Toggweiler, J. R., Wright, J. D., Katz, M. E., and Miller, K. G.: Ocean overturning since the late cretaceous: Inferences from a new benthic foramniniferal isotope compilation, Paleoceanography, 24, PA4216, doi:10.1029/2008PA001683, 2009.

De Boer, B., Van de Wal, R. S. W., Bintanja, R., Lourens, L. J., and Tuenter, E.: Cenozoic global ice-volume and temperature simulations with 1-D ice-sheet models forced by benthic δ^{18}O records, Ann. Glaciol., 51, 23–33, 2010.

De Boer, B., Van de Wal, R. S. W., Lourens, L. J., and Bintanja, R.: Transient nature of the Earth's climate and the implications for the interpretation of benthic δ^{18}O records, Palaeogeogr. Palaeocl., doi:10.1016/j.palaeo.2011.02.001, in press, 2011.

DeConto, R. M. and Pollard, D.: A coupled climate-ice sheet modeling approach to the early Cenozoic history of the Antarctic ice sheet, Palaeogeogr. Palaeocl., 198, 39–52, 2003.

DeConto, R. M., Pollard, D., Wilson, P. A., Pälike, H., Lear, C. H., and Pagani, M.: Thresholds for Cenozoic bipolar glaciation, Nature, 455, 652–656, 2008.

Diester-Haass, L., Billups, K., and Emeis, K.: Enhanced paleoproductivity across the Oligocene/Miocene boundary as evidenced by benthic foraminiferal accumulation rates, Palaeogeogr. Palaeocl., 302, 464–473, 2011.

Flower, B. P., Zachos, J. C., and Martin, E.: Latest Oligocene through early Miocene isotopic stratigraphy and deep-water paleoceanography of the western equatorial Atlantic: Sites 926 and 929, in: Proceedings of the Ocean Drilling Program, Scientific Results, edited by: Shackleton, N. J., Curry, W. B., Richter, C., and Bralower, T. J., 451–461, 1997a.

Flower, B. P., Zachos, J. C., and Paul, H.: Milankovitch-scale climate variability recorded near the oligocene/miocene boundary, in: Proceedings of the Ocean Drilling Program, Scientific Results., edited by: Shackleton, N. J., Curry, W. B., Richter, C., and Bralower, T. J., 433–439, 1997b.

Grinsted, A., Moore, J. C., and Jevrejeva, S.: Application of the cross wavelet transform and wavelet coherence to geophysical time series, Nonlin. Processes Geophys., 11, 561–566, doi:10.5194/npg-11-561-2004, 2004.

Hodell, D. A. and Woodruff, F.: Variations in the strontium isotopic ratio of seawater during the Miocene: stratigraphic and geochemical implications, Paleoceanography, 9, 405–426, 1994.

Kürschner, W. M., Kvacek, Z., and Dilcher, D. L.: The impact of Miocene atmospheric carbon dioxide fluctuations on climate and the evolution of terrestrial ecosystems, P. Natl. Acad. Sci. USA, 105, 449–453, 2008.

Laskar, J., Robutel, P., Joutel, F., Gastineau, M., Correia, A. C. M., and Levrard, B.: A longterm numerical solution for the insolation quantities of the Earth, Astron. Astrophys., 428, 261–285, 2004.

Lear, C. H., Rosenthal, Y., Coxall, H. K., and Wilson, P. A.: Late Eocene to early Miocene ice sheet dynamics and the global carbon cycle, Paleoceanography, 19, PA4015, doi:10.1029/2004PA001039, 2004.

Lisiecki, L. E. and Lisiecki, P. A.: Application of dynamic programming to the correlation of paleoclimate records, Paleoceanography, 17(4), 1049, doi:10.1029/2001PA000733, 2002.

Lourens, L. J. and Hilgen, F. J.: Long-periodic variations in the Earth's obliquity and their relation to third-order eustatic cycles and late Neogene glaciations, Quatern. Int., 40, 43–52, 1997.

Lourens, L., Hilgen, F., Shackleton, N. J., Laskar, J., and Wilson, D.: The Neogene period, in: A Geologic Time Scale 2004, edited by: Gradstein, F., Ogg, J., and Smith, A., Cambridge University Press, Cambridge, New York, Melbourne, 2004.

Miller, K. G. and Fairbanks, R. G.: Evidence for Oligocene-middle Miocene abyssal circulation changes in the Western North Atlantic, Nature, 306, 250–253, 1983.

Miller, K. G., Wright, J. D., and Fairbanks, R. G.: Unlocking the ice house: Oligocene-Miocene oxygen isotopes, eustacy and margin erosion, J. Geophys. Res., 96, 6829–6848, 1991.

Oslick, J. S., Miller, K. G., Feigenson, M. D., and Wright, J. D.: Oligocene-Miocene strontium isotopes: stratigraphy revisions and correlations to an inferred glacioeustatic record, Paleoceanography, 9, 427–443, 1994.

Pälike, H., Frazier, J., and Zachos, J. C.: Extended orbitally forced palaeoclimatic records from the Equatorial Atlantic Ceara Rise, Quaternary Sci. Rev., 25, 3138–3149, 2006a.

Pälike, H., Norris, R. D., Herrle, J. O., Wilson, P. A., Coxall, H. K., Lear, C. H., Shackleton, N. J., Tripati, A. K., and Wade, B. S.: The heartbeat of the Oligocene climate system, Science, 314, 1894–1898, 2006b.

Pagani, M., Arthur, M. A., and Freeman, K. H.: Miocene evolution of atmospheric carbon dioxide, Paleoceanography, 14, 273–292, 1999.

Paillard, D., Labeyrie, L., and Yiou, P.: Macintosh program performs time-series analysis, Eos Trans. AGU, 77, 379, 1996.

Paul, H. A., Zachos, J. C., Flower, B. P., and Tripati, A.: Orbitally induced climate and geochemical variability across the Oligocene/Miocene boundary, Paleoceanography, 15, 471–485, 2000.

Pekar, S. F. and DeConto, R. M.: High-resolution ice-volume estimates for the early Miocene: Evidence for a dynamic ice sheet in Antarctica, Palaeogeogr. Palaeocl., 231, 101–109, 2006.

Schlitzer, R.: Ocean data view 4, version 4.3.6, available at: http://odv.awi.de, last access: November 2010.

Shackleton, N. J.: Attainment of isotope equilibrium between ocean water and the benthonic foraminifera genus *uivergerina*: isotopic changes in the ocean during the last glacial, Colloq. Int. Ctr. National Rech. Sci., 219, 203–209, 1974.

Shackleton, N. J., Hall, M. A., Raffi, I., Tauxe, L., and Zachos, J. C.: Astronomical calibration age for the Oligocene-Miocene boundary, Geology, 28, 447–450, 2000.

Torrence, C. and Compo, G. P.: A practical guide to wavelet analysis, B. Am. Meteorol. Soc., 79, 61–78, 1998.

Van Dam, J. A., Abdul Aziz, H., Angeles Alvarez Sierra, M., Hilgen, F. J., van den Hoek Ostende, L. W., Lourens, L. J., Mein, P., van der Meulen, A. J., and Pelaez-Campomanes, P.: Long-period astronomical forcing of mammal turnover, Nature, 443, 687–691, 2006.

Von der Heydt, A. and Dijkstra, H. A.: Effect of ocean gateways on the global ocean circulation in the late Oligocene and early Miocene, Paleoceanography, 21, PA1011, doi:10.1029/2005PA001149, 2006.

Wade, B. S. and Pälike, H.: Oligocene climate dynamics, Paleoceanography, 19, PA4019, doi:10.1029/2004PA001042, 2004.

Woodruff, F. and Savin, S. M.: Miocene deepwater oceanography, Paleoceanography, 4, 87–140, 1989.

Wright, J. D. and Miller, K. G.: Miocene stable isotope stratigraphy, site 747, Kerguelen plateau, in: Proceedings of the Ocean Drilling Program, Scientific Results, Vol. 120, edited by: Wise Jr., S. W., Schlich, R., et al., College Station, TX, 855–866, 1992.

Wright, J. D., Miller, K. G., and Fairbanks, R. G.: Early and middle Miocene stable isotopes: implications for deepwater circulation and climate, Paleoceanography, 7, 357–389, 1992.

Zachos, J. C., Flower, B. P., and Paul, H. A.: Orbitally paced climate oscillations across the Oligocene/Miocene boundary, Nature, 388, 567–570, 1997.

Zachos, J. C., Pagani, M., Sloan, L., Thomas, E., and Billups, K.: Trends, rhythms, and aberrations in global climate 65 ma to present, Science, 292, 686–693, 2001a.

Zachos, J. C., Shackleton, N. J., Revenaugh, J. S., Pälike, H., and Flower, B. P.: Climate response to orbital forcing across the Oligocene-Miocene boundary, Science, 292, 274–278, 2001b.

Zachos, J. C., Kroon, D., and Blum, P., Shipboard Scientific Party: Proc. ODP, Init. Repts., 208, Ocean Drilling Program, College Station, TX doi:10.2973/odp.proc.ir.208.2004, 2004.

Zachos, J. C., Dickens, G. R., and Zeebe, R. E.: An early Cenozoic perspective on greenhouse warming and carbon-cycle dynamics, Nature, 451, 279–283, 2008.